Catalysis Today 171 (2011) 290–296

Contents lists available at ScienceDirect

Catalysis Today

journal homepage: www.elsevier.com/locate/cattod

A comparison between copper and nickel-based catalysts obtained from hydrotalcite-like precursors for WGSR

Edgardo Meza Fuentes[a,b], Arnaldo da Costa Faro Júnior[c], Tatiana de Freitas Silva[d], José Mansur Assaf[d], Maria do Carmo Rangel[a,*]

[a] GECCAT Grupo de Estudos em Cinética e Catálise, Instituto de Química, Universidade Federal da Bahia, Campus Universitário de Ondina, Federação, 40 170-280, Salvador, Bahia, Brazil
[b] Grupo de Estudios en Materiales y Combustibles, Facultad de Ciencias Exactas y Naturales, Universidad de Cartagena, Colombia
[c] Universidade Federal do Rio de Janeiro, Ilha do Fundão, 21941-909, Rio de Janeiro, Rio de Janeiro, Brazil
[d] Universidade Federal de São Carlos, Rod. Washington Luiz, Km 235, 13565-905, São Carlos, São Paulo, Brazil

ARTICLE INFO

Article history:
Received 3 November 2010
Received in revised form 3 March 2011
Accepted 29 March 2011
Available online 1 June 2011

Keywords:
Hydrotalcites
Nickel
Copper
Aluminum
WGSR
Hydrogen

ABSTRACT

Nickel or copper-based catalysts were obtained from hydrotalcite-like precursors in this work, in order to find catalysts able to work at intermediates temperatures (200–350 °C) in water gas shift reaction (WGSR). Samples based on nickel (or copper), aluminum and zinc were obtained by co-precipitation, characterized by several techniques and evaluated in WGSR. Zinc caused changes in the cell parameters of hydrotalcite-type structure, which determined the structural and textural properties of calcined samples. For all catalysts, zinc oxide was detected. In the case of nickel-based hydrotalcites, aluminum cations were incorporated into nickel oxide lattice, hindering reduction; however, the addition of zinc decreased this effect. For copper-based samples, aluminum entered into copper oxide lattice and the copper reduction decreased with the increase of zinc amount in solids. After calcination, copper catalysts showed lower specific surface areas than nickel ones. Zinc led to the production of smaller and more reducible nickel oxide particles, due to the decrease of their interaction with Al^{3+} species; under reduction, they produced small metallic nickel particles, which are supposed to be highly active and selective to carbon dioxide. Copper catalysts were less active to WGSR, as compared to the nickel ones, this can be related to their low specific surface areas. All catalysts were active in the range of 200–350 °C and thus are candidates to be used in a single stage of WGSR at intermediate temperatures.

1. Introduction

For several years, the water gas shift reaction (WGSR) has been one of the most important steps in industrial production of pure hydrogen [1,2]. In recent times, the environmental problems related to the use of fossil fuels, as well as the development of new technologies for energy generation from hydrogen, have increased the interest for the WGSR even more, especially because of its role in fuel cells [3,4].

In the production of high pure hydrogen, the WGSR is used for removing carbon monoxide produced in natural gas reforming and for increasing hydrogen production. In commercial processes, the reaction is normally performed in two steps, in order to achieve rates for industrial applications. The first one is carried out at high temperatures over iron oxide-based catalysts and is known as high temperature shift (HTS), while the second step is performed at low temperatures over copper-based catalysts (low temperature shift, LTS) [1,2,5]. In spite of these two steps have been used for many years, there is an interest for developing catalysts active enough to carry out the process in only one step at intermediates temperature, decreasing the operational costs.

The traditional chromium-based hematite catalyst, used in the high temperature shift step, works in the range of 350–450 °C and has several advantages such as high activity, low cost and resistance against several poisons [1,6]. The last generation of the HTS catalysts also contains copper, which improved the performance even more, by increasing the activity [7–9]. However, the activity of both catalysts significantly decreases with temperature, making them unable to operate at temperatures lower than 350 °C.

On the other hand, the copper-based catalysts operate in the range of 180–250 °C in the LTS step and are susceptible to poisoning and sintering [1,2]. It is well-known [1] that they are not able

* Corresponding author. Tel.: +55 7132836867; fax: +55 7132836867.
E-mail address: mcarmov@ufba.br (M.d.C. Rangel).

0920-5861/$ – see front matter © 2011 Elsevier B.V. All rights reserved.
doi:10.1016/j.cattod.2011.03.082

to work at temperatures higher than 250 °C, because the activity rapidly decreases due to copper sintering [1,2,10].

Therefore, there is a need of developing new catalysts for operating at intermediate temperatures in water gas shift reaction. Several modified iron-based catalysts and copper-based ones were evaluated in the reaction [1,11–15], as well as new ones [1,16–20], for both high and low temperature shift steps. Especially cobalt, ceria and nickel-based catalysts have been shown high performances [16,19,20]. However, even these catalysts have not shown enough activity at intermediate temperatures to be considered as a potential system to perform WGSR in a single step.

In a previous work [16], it was found that lanthana-supported nickel catalysts are promising systems for WGSR, at 370 °C. Also, the addition of small amounts of aluminum increased the specific surface area and the activity and thus this dopant is beneficial to the catalyst. In the present work, nickel-based catalysts obtained from hydrotalcites were obtained in order to develop new catalysts for WGSR carried out at intermediate temperatures. For comparison purposes, copper-based catalysts were also prepared and evaluated in WGSR in the same conditions.

In recent times, hydrotalcite-like compounds have been attracted much attention as catalyst precursors since it was demonstrated that they are optimal precursors for hydrogenation catalysts [21]. Upon heating, they decompose to a mixed oxide of high specific surface area, with chemical homogeneity and strong Lewis basic sites [22,23], being suitable catalysts for several base-catalyzed reaction [21,23–25]. These homogeneous mixtures of oxides with very small crystal size, produced during calcination, are thermally stable and form stable metal crystallites by reduction [21]. In addition, when the calcined hydrotalcite is brought into contact with water solutions containing several anions, the original structure is reconstructed, giving rise to the so called memory effect [21].

Hydrotalcites have the structure $[M(II)_{1-x}M(III)_x(OH)_2](A_{x/n}{}^{n-})\cdot mH_2O$, where M(II) is a divalent cation such as magnesium, nickel, zinc, cobalt or copper, while M(III) is a trivalent cation such as aluminum, chromium and iron, among others, with $A_{x/n}{}^{n-}$ as an anion of charge n such as $CO_3{}^{2-}$, NO^{3-}, Cl^-, $SO_4{}^{2-}$ and others. Its structure resembles that of brucite, $Mg(OH)_2$, in which magnesium cations are octahedrally coordinated by hydroxyl ions, resulting in stacks of edge-shared layers of octahedra. When the magnesium cations are replaced by a trivalent ion with similar ration (such as Al^{3+}) a positive charge is generated in the hydroxyl sheet. This net positive charge is compensated by $(CO_3)^{2-}$ anions, which is located between two brucite-like sheets. Furthermore, water of crystallization is present in the interlayer [21].

2. Experimental

2.1. Catalysts preparation

Samples were prepared by the low supersaturating method at constant pH, by preparing a solution containing aluminum nitrate ($Al(NO_3)_3\cdot 9H_2O$), zinc nitrate ($Zn(NO_3)_2\cdot 6H_2O$) and nickel (or copper) nitrate, $Ni(NO_3)_2\cdot 6H_2O$ or $Cu(NO_3)_2\cdot 6H_2O$ and another solution containing potassium hydroxide and potassium carbonate. Both solutions were added in different streams simultaneously, through a peristaltic pump, to a beaker with water (400 mL), under vigorous stirring keeping pH at 8.3. The resulting mixture was aged at 65–70 °C, for 2 h. The solid obtained was separated by filtration and washed with distillate water up to remove the nitrate ions. The samples were then dried at 60 °C, for 24 h and calcined under flow air (100 mL min^{-1}) at 500 °C, for 4 h. For all samples the M^{2+}/Al ratio was equal to 2 and the Ni (Cu)/Zn ratios were of 2 and 1, respectively.

2.2. Samples characterization

The solids were characterized by atomic absorption spectroscopy, thermogravimetry, X-ray diffraction, Fourier transform infrared spectroscopy, Raman spectroscopy, specific surface area and porosity measurements, temperature-programmed reduction and copper dispersion measurements.

Elemental chemical analyses were carried out by atomic absorption spectroscopy (AAS) on a Unicam 969 Solar instrument. For this analysis, the samples were previously dissolved in acid medium, using a mixture of nitric acid and hydrochloric acid. The experiments of thermogravimetry (TG) were performed in a TA Instruments SDT 2670. The samples (0.015 g) were heated at 10 °C min^{-1} from 25 to 800 °C range, under air flow of 50 mL min^{-1}.

The X-ray diffraction (XRD) patterns of precursors and calcined solids were recorded in a Shimadzu XDR-600 with CuKα radiation (λ = 1.54059 Å) generated at 40 kV and 40 mA, using at 0.02 step size at the room temperature, in the 5–80° (2θ) range. The X-ray diffraction patterns of the spent catalysts were recorded in Rigaku Multiflex, with CuKα radiation (λ = 1.54059 Å), generated at 40 kV and 40 mA. The cell parameters of hydrotalcite were calculated by XPowder software, using the interplanar spacings of (1 1 0) and (0 0 3) planes for a and c cell parameters, respectively, considering a unit cell belonging to the rhombohedral R-3m system. The cell parameters and the average particles size were calculated using (2 0 0) and (1 1 1) planes for nickel oxide and copper oxide, respectively, by applying the Lorentz model and the Scherrer equation. For calculating the cell parameters, the cubic system with Fm-3m symmetry and the monoclinic system with C2/c spatial group were considered for nickel oxide and copper oxide, respectively.

Fourier transform infrared spectroscopy (FTIR) analyses were performed in a Perkin Elmer model Spectrum One, using samples diluted in potassium bromide discs with a 1:100 ratio. The spectra were recorded in the region between 4000 and 400 cm^{-1}, using 32 scan and a resolution of 4 cm^{-1}. Raman spectra were obtained in a LabRAM HR-UV 800/Jobin-Yvon apparatus, equipped with two lasers He–Ne (l = 632 nm) and Ar (l = 514 nm), with a resolution of 1 mm^3, focusing the samples in a optical microscope with objectives of 10×, 50× and 100×, using a CCD detector at −70 °C. Samples were analysed as self-supported discs.

The specific surface area (Sg) and porosity of the calcined solids were measured by nitrogen adsorption/desorption at −196.15 °C by BET and BJH methods, respectively, using a Micromeritics ASAP 2010 instrument. Before the analysis, the sample (0.2 g) was heated up to 200 °C under vacuum (2 μm Hg) to remove water from the solids. The temperature-programmed reduction analyses were carried in a Zeton Altamar AMI 90 equipped with a TCD detector. Before the analysis the samples (0.05 g) were heated up to 300 °C in order to remove water and then cooled to 25 °C. During analyses, the samples were heated from 25 to 1000 °C in the case of nickel-based solids and from 25 to 800 °C for copper-based solids, under a flow (50 mL min^{-1}) of a 5% H_2/Ar mixture.

For copper dispersion and metallic area measurements, the samples were reduced under a flow of a 5% H_2/N_2 mixture, from room temperature to 350 °C, under a heating rate of 10 °C min^{-1} and kept at this temperature for 1 h, by monitoring the hydrogen consumption. The condition of reduction used in this step is the same as that one used in the reduction of copper catalysts before the catalytic tests. The solids were then cooled to 90 °C and oxidized with nitrous oxide in a flow of 30 mL min^{-1}, for 80 min. The ratio of hydrogen consumption before and after oxidation with nitrous oxide provided copper dispersion. The metallic area of copper of the solids

Table 1
Number of moles and metal molar ratios and CO_3^{2-} anion per 100 g of precursor.

Sample	Ni	Cu	Zn	Al	CO_3^{2-}	Ni/Zn	Ni/Al	Cu/Zn	Cu/Al
$N_{0.66}A_{0.33}$	0.65	–	–	0.30	0.15	–	2.16	–	–
$N_{0.44}Z_{0.22}A_{0.33}$	0.45	–	0.22	0.32	0.15	2.15	1.40	–	–
$N_{0.33}Z_{0.33}A_{0.33}$	0.33	–	0.30	0.30	0.15	1.10	1.10	–	–
$C_{0.44}Z_{0.22}A_{0.33}$	–	0.46	0.22	0.32	0.16	–	–	2.09	1.40
$C_{0.33}Z_{0.33}A_{0.33}$	–	0.31	0.31	0.30	0.15	–	–	1.00	1.03

is calculated by the number of copper atoms per unit surface area, 1.47×10^{19} atom Cu/m^2 [26].

2.3. Catalysts evaluation

The catalysts were evaluated in WGSR in the 200–350 °C range. Before reaction, nickel-based solids were reduced in situ, at 500 °C, for 2 h, under hydrogen flow. Copper-based solids were also reduced previously in situ, at 350 °C, during 1 h under a flow of 10% H_2/N_2 mixture. The gaseous effluent was analysed by on line gas chromatography, using a Varian Model 3800 instrument, equipped with 2 TCD detectors.

The catalyst performance was evaluated using 0.1 g of powder and a fixed bed microreactor consisting of a stainless tube. All experiments were carried at atmospheric pressure, under a flow (60 mL min^{-1}) of a gas mixture with composition of 10% CO and 90% N_2. A steam to carbon monoxide ratio equal to 10 was used for all runs. The steam used was generated through the addition of water by a bomb to a vaporizer at 303 °C. After reaction, the catalysts were characterized by X-ray diffraction.

3. Results and discussion

The results of chemical analysis are shown in Table 1. It can be noted that the number of moles obtained for all the samples are very close to the expected values. Also, the amount of carbonate anions is around half the quantity of Al^{3+} cations for all cases, as expected for hydrotalcites in which the amount of bivalent anions is half the amount of trivalent cations. These results show that the co-precipitation method, in low saturation at constant pH, is suitable for preparing nickel and copper-based hydrotalcites with the expected compositions.

The hydrotalcite structure (JCPDS 89-0460) was found for all samples, as shown in Fig. 1. Nickel-based solids showed similar XRD patterns but there was a shift of the (1 1 0) peak to lower angles due to the addition and increase of zinc content, this is possibly due to the higher radius of Zn^{2+} species as compared to the Ni^{2+} and Al^{3+} ones; this led to an increase of the *a* cell parameter, as shown in Table 2, in agreement with previous work [21]. In the case of copper-based materials, the solid with the highest zinc content ($C_{0.33}Z_{0.33}A_{0.33}$) originated a diffractogram with larger number of peaks which are narrower, showing that this solid is made up of a more organized hydrotalcite structure, as compared to the other solids. The difference noted in the *c* parameter for the $C_{0.44}Z_{0.22}A_{0.33}$ sample (Table 2) is possibly due to the highest content of carbonate (Table 1), which increased the electrostatic interaction between the carbonate anions and the positive layers, decreasing the value of *c* parameter.

Table 2
Values of cell parameters of hydrotalcites.

Sample	*a* parameter (Å)	*c* parameter (Å)
$N_{0.66}A_{0.33}$	3.030	22.908
$N_{0.44}Z_{0.22}A_{0.33}$	3.041	22.750
$N_{0.33}Z_{0.33}A_{0.33}$	3.048	22.750
$C_{0.44}Z_{0.22}A_{0.33}$	3.032	21.810
$C_{0.33}Z_{0.33}A_{0.33}$	3.074	22.630

The infrared spectra of hydrotalcites are shown in Fig. 2. The broad band observed at 3400–3600 cm^{-1}, for all solids, is characteristic of the ν (O–H) stretching vibration of water molecules in the interlayer region and of hydroxyl groups of positive layers [27,28]. The carbonate anions originated bands at 1368 cm^{-1} (ν_3 stretching), 1060 cm^{-1} (ν_1 stretching) and 870 cm^{-1} (ν_2 stretching) [27–30]. The carbonate anions in interaction with water molecules also produced a signal between 3000 and 3100 cm^{-1} for all solids. In the case of $C_{0.44}Z_{0.22}A_{0.33}$ sample, it was observed a band at 1525 cm^{-1} originated by the interaction between carbonate and hydroxyl anions, possibly due to the smaller distance between the

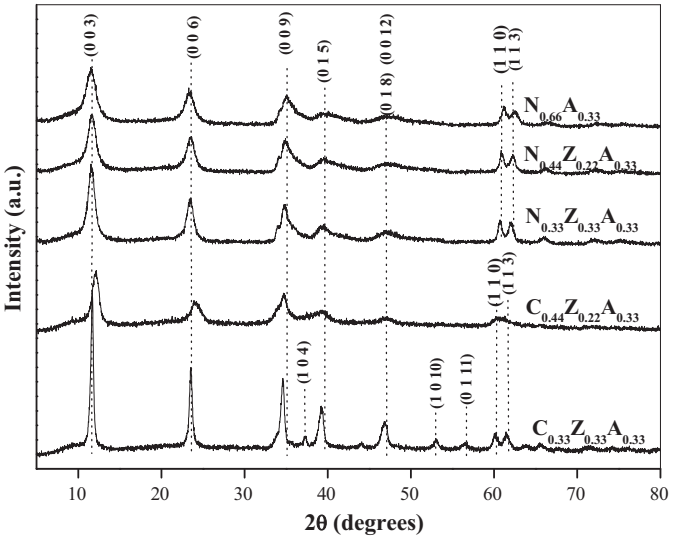

Fig. 1. X-ray diffractograms of nickel or copper-based hydrotalcites.

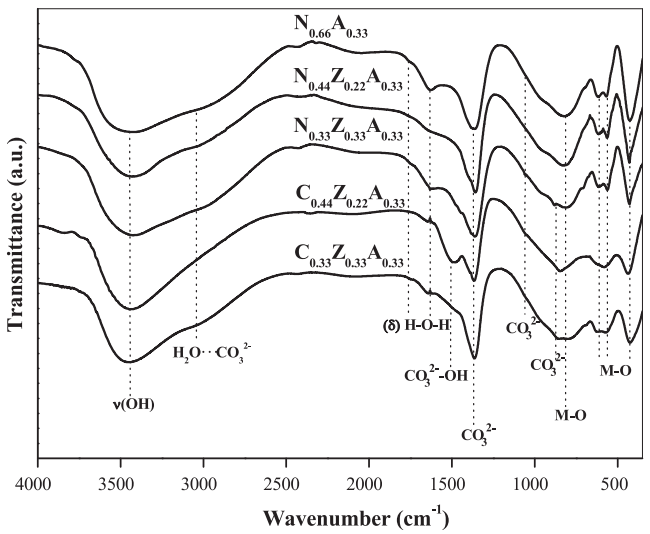

Fig. 2. FTIR spectra of nickel or copper-based hydrotalcites.

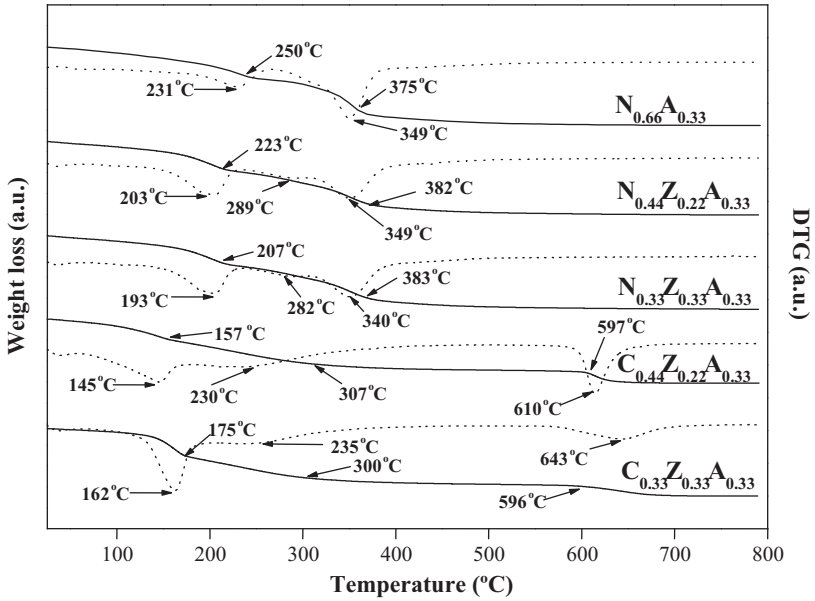

Fig. 3. Thermogravimetry curves of nickel or copper-based hydrotalcites.

positive layers, which is evidenced by the lower value of *c* parameter for this material.

The thermogravimetry curves of hydrotalcites showed similar behaviors upon heating, with three stages of weight loss, as shown in Fig. 3. For the nickel and aluminum-based solid ($N_{0.66}A_{0.33}$ sample), the first step occurred in the range of 30–250 °C and 14.92% weight was lost, which corresponds to the exit of water molecules located between the layers [21]. After this, there is a plateau, indicating the beginning of the collapse of the hydrotalcite structure, which causes a decrease of space between the layers and makes the exit of water molecules more difficult [31]. A second weight loss (17.51%) is noted, from 350 to 375 °C, which corresponds to the total collapse of the structure and the beginning of the oxide formation, this process is followed by the exit of hydroxyls groups. The last stage, at higher temperatures, corresponds to the loss (37.06%) of carbonate groups occluded in the structure [32]. The introduction of zinc in the hydrotalcite caused a shift of the weight loss to lower temperatures, indicating that it decreased the structure stability; this effect increased with zinc amount.

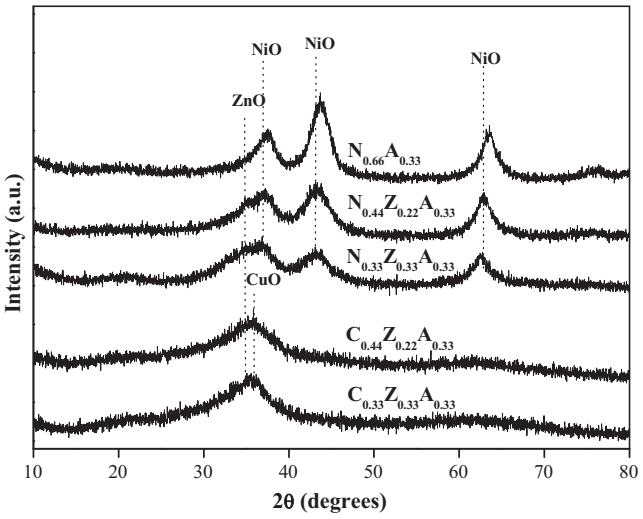

Fig. 4. X-ray diffractograms of calcined nickel or copper-based hydrotalcites.

It can be observed that copper-based hydrotalcites are thermally less stable then the nickel-based ones (Fig. 3). In the first case, the collapse occurred at temperatures below 200 °C, possibly due to the formation of copper oxide (CuO), which is typically produced at temperatures higher than 150 °C [33] and then decreased the stability of hydrotalcite structure. The weight loss observed at temperatures close to 600 °C is due to the decomposition of carbonate anions that were trapped during the collapse and can form carbonates with the cations present in the original structure [34,35].

From the X-ray diffractograms of the calcined solids based on aluminum and nickel, one can see only the presence of nickel oxide (NiO, JCPDS 04-0835), as shown in Fig. 4. It was observed (Table 3) that the *a* cell parameter of nickel oxide in solids is lower than the reported value, this means that some Al^{3+} cations entered into the cubic lattice of nickel oxide reducing its cell dimensions, because of the smaller radius of Al^{3+} species (0.53 Å), as compared to Ni^{2+} ones (0.69 Å), in agreement with previous works [21,36,37]. On the other hand, the addition of zinc increased the *a* cell parameter of nickel oxide in solids, suggesting that some Zn^{2+} cations entered into the nickel oxide lattice, causing an increase in the cell dimensions, due to the higher ionic radius of Zn^{2+} species (0.74 Å), as compared to Ni^{2+} ones. However, the presence of zinc oxide was also noted, for both samples ($N_{0.44}Z_{0.22}A_{0.33}$ and $N_{0.33}Z_{0.33}A_{0.33}$). For copper-based samples, only an amorphous halo was noted in X-ray diffractograms, as shown in Fig. 4, which can be assigned to copper oxide.

The presence of zinc in the nickel-based solids led to higher dispersion of nickel oxide particles, as shown in Table 3, this effect increased with the amount of zinc in solids. This finding can be related to the role of zinc oxide in making nickel oxide particles

Table 3
Values of *a* parameter of cubic cell, cell volume and particle size of nickel oxide (NiO) formed during calcination of hydrotalcites.

Sample	Parameter *a* (Å)	Cell volume (Å)	Particle size (nm)
NiO[a]	4.16	71.99	–
$N_{0.66}A_{0.33}$	4.14	70.95	3.02
$N_{0.44}Z_{0.22}A_{0.33}$	4.17	72.51	1.96
$N_{0.33}Z_{0.33}A_{0.33}$	4.19	73.65	1.53

[a] Data obtained from (04-0835) JCPDS card.

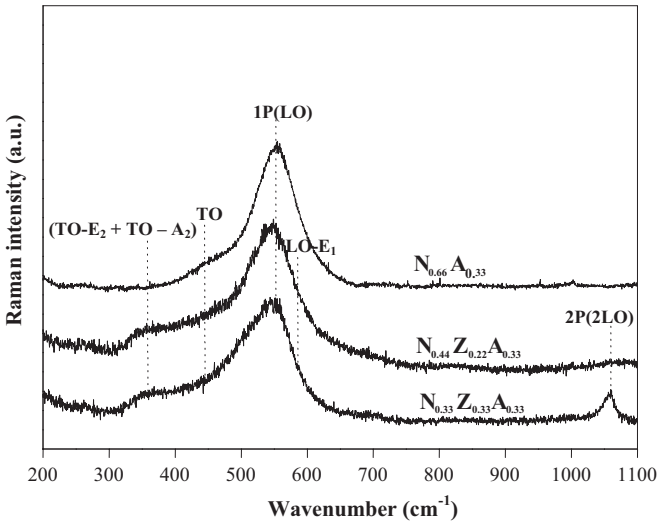

Fig. 5. Raman spectra of nickel-based hydrotalcites after calcination.

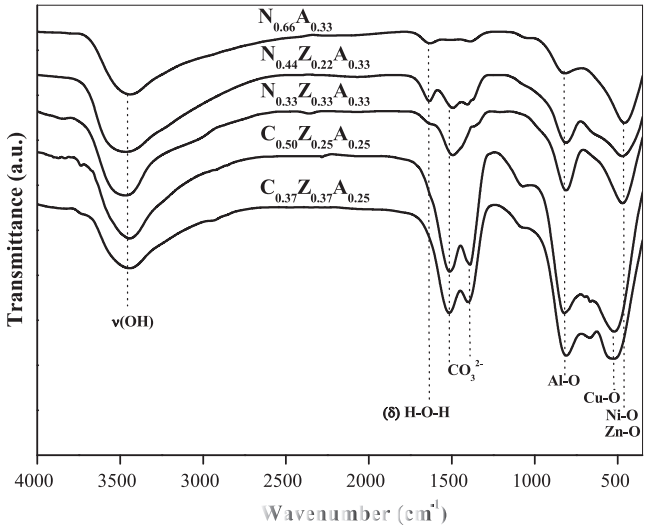

Fig. 7. FTIR spectra of calcined nickel or copper-based hydrotalcites.

apart, hindering agglomeration and subsequent growth of those particles.

The Raman spectra (Figs. 5 and 6) confirmed the presence of zinc oxide for all calcined solids. In nickel-containing samples, zinc oxide originated a band between 300 and 400 cm^{-1}, due to the overlapping of TO–E_2 (336 cm^{-1}) and TO–A_1 (381 cm^{-1}) modes of the hexagonal structure of zinc oxide, ZnO [38]. In these spectra, the bands of nickel oxide corresponding to the TO and LO (1P) modes were also observed [39–41]. In the spectra of $N_{0.44}Z_{0.22}A_{0.33}$ sample, a band attributed to LO + LO vibration was noted, which is typical of the cubic structure of nickel oxide with few imperfections [39–41]. For this solid, XRD showed that the cubic cell dimensions of nickel oxide formed during calcination of hydrotalcite were similar to nickel oxide from literature (Table 2), indicating that zinc decreased the amount of Al^{3+} species in nickel oxide lattice. The Raman spectra of copper-based solids, after calcination, confirmed the presence of copper oxide (CuO), by the bands the bands corresponding to the A_g and $2B_g$ modes of the monoclinic structure of the CuO [42,43].

The infrared spectra of the samples showed similar profiles, as shown in Fig. 7. The presence of carbonate anions in the calcined material was detected mainly for copper-based materials. These anions remained in these materials due to the collapse of the hydrotalcite structure at low temperatures, which causes the trapping of these species inside the solid. The infrared spectra confirmed also the presence of aluminum, copper and nickel species, by the bands at low wavenumbers, attributed to M–O stretching (M = metal) [44].

Table 4
Textural properties of calcined solids.

Sample	Sg (m^2/g)	Pore volume (cm^3/g)	Pore diameter (nm)
$N_{0.66}A_{0.33}$	200	0.50	4.2
$N_{0.44}Z_{0.22}A_{0.33}$	172	0.65	5.7
$N_{0.33}Z_{0.33}A_{0.33}$	182	0.48	6.4
$C_{0.44}Z_{0.22}A_{0.33}$	36	0.18	10.5
$C_{0.33}Z_{0.33}A_{0.33}$	33	0.16	10.4

Aluminum and nickel-based samples showed the highest specific surface areas, while copper-containing solids showed the lowest ones, as shown in Table 4. From the nitrogen isotherms (not shown) it was found that the nickel-based solids were macroporous with some mesopores, while the copper-based ones were macroporous.

Nickel-based solids showed similar TPR curves with a broad peak from 300 to 800 °C (Fig. 8). By deconvolution, several peaks

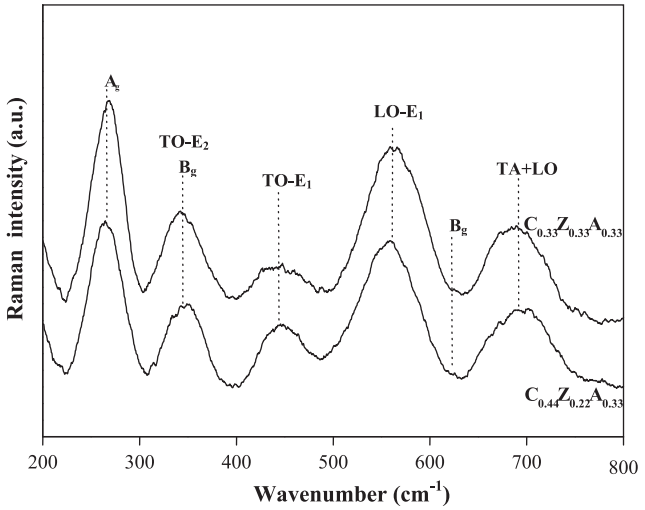

Fig. 6. Raman spectra of copper-based hydrotalcites after calcination.

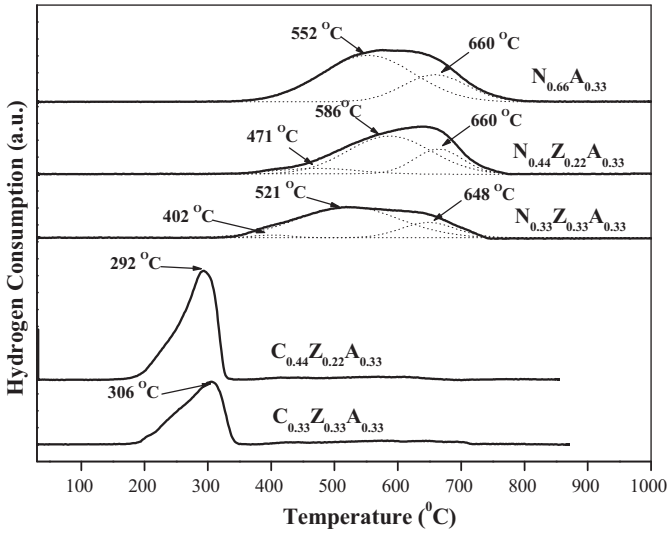

Fig. 8. TPR curves of calcined nickel or copper-based hydrotalcites.

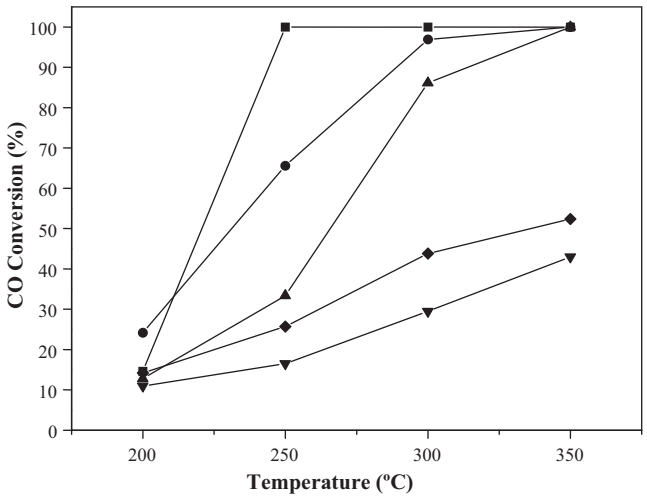

Fig. 9. Conversion of carbon monoxide over nickel or copper catalysts as a function of reaction temperature. $N_{0.66}A_{0.33}$ (–■–); $N_{0.44}Z_{0.22}A_{0.33}$ (–●–); $N_{0.33}Z_{0.33}A_{0.33}T$ (–▲–); $C_{0.44}Z_{0.22}A_{0.33}$ (–▼–); $C_{0.33}Z_{0.33}A_{0.33}$ (–♦–).

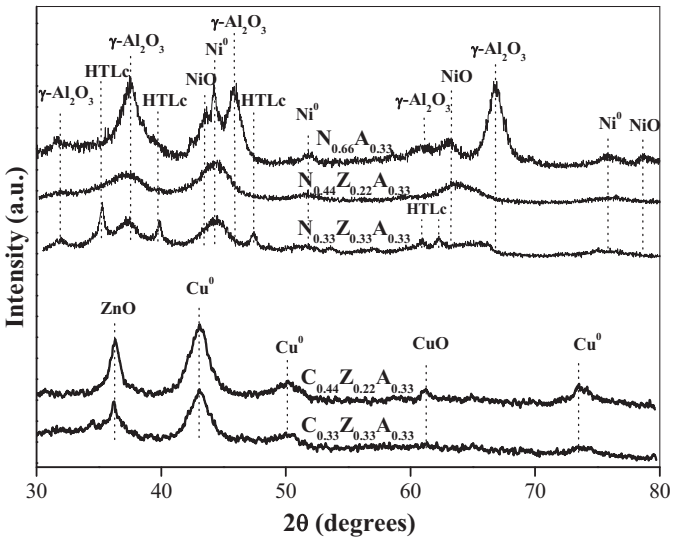

Fig. 10. X-ray diffractograms of spent catalysts produced by calcination of nickel or copper-based hydrotalcites.

were obtained related to the reduction of nickel in several kinds of interactions with the support. Regarding the nickel and aluminum-based sample, the deconvolution produced two peaks, the first one (around 520 °C) can be assigned to the reduction of nickel containing Al^{3+} species in the lattice, causing an increase of the temperature required to reduce this oxide [21,45]. The peak at higher temperature is probably associated with a transition phase to nickel aluminate or by nickel oxide particles in strong interaction with aluminum amorphous phases, in agreement with previous work [46]. One can note that the addition of zinc shifted the peak to lower temperatures, indicating a decrease of the interaction between nickel and the support caused by zinc, the increase of zinc amount increased this effect even more. This finding can be related to the decrease of Al^{3+} ions in the lattice, as zinc is being incorporated. The deconvolution of these curves indicates three different kinds of interactions of nickel oxide particles with the support, in accordance with other works [45]. As compared to nickel and aluminum-based sample, these curves showed an additional peak at low temperatures, associated to nickel oxide particles in weak interaction with the support.

As expected, copper particles were more susceptible to reduction than nickel ones; in addition, the interaction between copper and the support increased with zinc amount. Copper-based solids showed a single reduction peak, assigned to the reduction of copper oxide, CuO, to produce Cu^0 species. The maximum for the reduction peak appeared at lower temperature for the $C_{0.44}Z_{0.22}A_{0.33}$ sample, as compared to $C_{0.33}Z_{0.33}A_{0.33}$ one. In agreement with these findings, the first sample showed the highest dispersion (25%,) and then the metallic area (25 $m^2\ g^{-1}$) while the other $C_{0.33}Z_{0.33}A_{0.33}$ sample, which showed the lowest dispersion and metallic area (22%; 15 m^2/g).

All solids were active in WGSR in the range of 200–350 °C and the activity increased with temperature (Fig. 9). The aluminum and nickel-based catalyst ($N_{0.66}A_{0.33}$ sample) was the most active one, achieving 100% of carbon monoxide conversion at 250 °C. However, it produced methane in this temperature range, and this effect increased with temperature, as shown in Table 5. By adding different amounts of zinc to this catalyst, the methane production was inhibited and the catalysts achieved 100% of selectivity for all temperature range; however, this addition caused a decrease in conversion. On the other hand, the activity increased with nickel content and then the lowest activity was shown by the $N_{0.33}Z_{0.33}A_{0.33}$ sample, among the nickel-based catalysts.

As a whole, copper-based catalysts are less active than the nickel-based ones, a fact which can be related to their lower specific surface areas. They were selective only towards carbon dioxide, the activity increased with temperature for all catalysts. For these samples, the difference in activity is not related to the metallic area of copper. The highest activity of $C_{0.33}Z_{0.33}A_{33}$ sample can be associated to the highest amount of zinc, which improved the catalytic activity of copper, by a synergistic effect, as reported previously [47].

After WGSR, all catalysts showed metallic nickel and aluminum oxide (γ-A_2O_3), as shown in Fig. 10, the last one was produced during reaction. The nickel and alumina-based catalyst also showed nickel oxide (NiO), a fact that can be related to the presence of aluminum, which makes nickel reduction more difficult [46]. The nickel and zinc-containing samples did not show nickel oxide, due to the action of zinc in favoring nickel reduction, as found by TPR. The $N_{0.33}Z_{0.33}A_{0.33}$ sample also showed peaks related to hydrotalcites, indicating that it has the memory effect, which was possible due to the presence of carbon dioxide and water during reaction.

Table 5
Methane selectivity (*S*) of the $N_{0.66}A_{0.33}$ catalyst at several temperatures.

Temperature (°C)	*S* (%)
350	4.0
300	2.0
250	2.0
200	0.0

4. Conclusions

Heating hydrotalcites based on nickel, aluminum and zinc produces nickel and zinc oxides with some aluminum dispersed in the lattice. This occurs at temperatures higher than those for copper, zinc and aluminum-based solids. Zinc favors the decomposition of nickel-based hydrotalcites while the opposite occurs for copper-based ones. Zinc decreases the reduction temperature for calcined nickel-based hydrotalcites and increases for copper-based ones. All catalysts based on calcined hydrotalcites are active in water gas shift reaction (WGSR) and selective to carbon dioxide. The sample based on nickel and aluminum is also selective to methane but the addition of zinc inhibits its production. The activity of nickel-based catalysts increases with the amount of nickel in solids while the activity of the copper-based ones increases with zinc amount

which improves the copper activity by a synergetic effect. The most promising catalyst for water gas shift reaction is the $N_{0.44}Z_{0.22}A_{0.33}$ sample, which shows the highest activity in the range of 200–350 °C and does not produce methane, being promising to be used in a single stage of WGSR at intermediate temperatures.

Acknowledgments

EMF thanks FAPESB for his scholarship. The authors thank CNPq and FINEP for the financial support.

References

[1] D.S. Newsome, Catal. Rev. Sci. Eng. 21 (1980) 275–318.
[2] L. Lloyd, D.E. Ridler, M.V. Twigg, The water gas shift reaction, in: M.V. Twigg (Ed.), Catalysis Handbook, Wolfe Scientific Books, London, 1996, pp. 283–339.
[3] L.W. Faria, L.C. Dieguez, M. Schmal, Appl. Catal. 85 (2008) 77–85.
[4] J.D. Holladay, J. Hu, D.L. King, Y. Wang, Catal. Today 139 (2009) 244–260.
[5] G.C. Araujo, M.C. Rangel, Stud. Surf. Sci. Catal. 130 (2000) 1601–1606.
[6] A.L.C Pereira, G.J.P. Berrocal, S.G. Marchetti, A. Albornoz, A.O. de Souza, M.C. Rangel, J. Mol. Catal. A: Chem. 281 (2008) 66–72.
[7] A.O. de Souza, M.C. Rangel, React. Kinet. Catal. Lett. 79 (2003) 175–180.
[8] E.B. Quadro, M.L.M. Dias, A.M.M. Amorim, M.C. Rangel, J. Braz. Chem. Soc. 10 (1999) 51–59.
[9] E.B. Quadro, M.O. Souza, M.C. Rangel, Quím. Nova 21 (1998) 428–433.
[10] A.O. de Souza, G.C. Araújo, E.A. Pinheiro, M.C. Rangel, Quím. Nova 25 (2002) 181–185.
[11] J.L.R. Costa, S.G. Marchetti, M.C. Rangel, Catal. Today 77 (2002) 205–213.
[12] G.C. Araújo, M.C. Rangel, Catal. Today 62 (2000) 201–207.
[13] I. Lima Jr., J. Millet, A. Mimoun, M.C. Rangel, Appl. Catal. A: Gen. 283 (2005) 91–98.
[14] A.L.C. Pereira, N.A. dos Santos, M.L.O. Ferreira, L.A.M. Albornoz, M.C. Rangel, Stud. Surf. Sci. Catal. 167 (2007) 225–230.
[15] M.C. Rangel, R.M. Sassaki, F. Galembeck, Catal. Lett. 33 (1995) 237–254.
[16] M.S. Santos, G.J.P. Berrocal, J.L.G. Fierro, M.C. Rangel, Stud. Surf. Sci. Catal. 167 (2007) 493–498.
[17] P. Querino, J.R.C. Bispo, M.C. Rangel, Catal. Today 108 (2005) 920–925.
[18] A.O. Souza, M.C. Rangel, O.L. Alves, Quím. Nova 28 (2004) 46–49.
[19] J.Y. Lee, D.W. Lee, K.Y. Lee, Y. Wang, Catal. Today 146 (2009) 260–264.
[20] T. Li, Q. Fu, M. Flytzani-Stephanopoulos, Appl. Catal. B: Environ. 27 (2000) 179–191.
[21] F. Cavani, F. Trifiro, A. Vaccari, Catal. Today 11 (1991) 173–301.
[22] J.L. Di Cosimo, V.K. Diez, M. Xu, E. Iglesia, C.R. Apesteguia, J. Catal. 178 (1998) 499–510.
[23] M.J. Climent, A. Corma, S. Iborra, J. Primo, J. Catal. 151 (1995) 60–66.
[24] V.R.L. Constantino, T.J. Pinnavaia, Catal. Lett. 23 (1994) 361–367.
[25] D.E. Laycok, R.J. Collacott, D.A. Skelton, M.F. Tchir, J. Catal. 130 (1991) 354–358.
[26] K.V.R. Chary, K.K. Seela, D. Naresh, P. Ramakanth, Catal. Commun. 9 (2008) 75–81.
[27] J.T. Kloprogge, D. Wharton, L. Hickey, R.L. Frost, Am. Mineral. 87 (2002) 623–629.
[28] N. Iyi, T. Matsumoto, Y. Kaneko, K. Kitamura, Chem. Mater. 16 (2004) 2926–2932.
[29] E.C. Kruissink, L.L. van Reijden, J.R.H. Ross, J. Chem. Soc., Faraday Trans. I 77 (1981) 649–663.
[30] S. Albertazzi, F. Basile, P. Benito, P. Del Gallo, G. Fornasari, D. Gary, V. Rosetti, A. Vaccari, Catal. Today 128 (2007) 258–263.
[31] A.H. Iglesias, O.P. Ferreira, D.X. Gouveia, A.G. Souza Filho, J.A.C. de Paiva, J. Mendes Filho, O.L. Alves, J. Solid State Chem. 178 (2005) 142–152.
[32] A. Alejandre, F. Medina, X. Rodriguez, P. Salagre, Y. Cesteros, J.E. Sueiras, Appl. Catal. B: Environ. 30 (2001) 195–207.
[33] Y. Cudennec, A. Lecerf, Solid State Sci. 5 (2003) 1471–1474.
[34] A. Alejandre, F. Medina, P. Salagre, X. Correig, J.E. Sueiras, Chem. Mater. 11 (1999) 939–948.
[35] N. Voyer, A. Soisnard, S.J. Palmer, W.N. Martens, R.L. Frost, J. Therm. Anal. Calorim. 96 (2009) 481–485.
[36] V. Rives, S. Kannan, J. Mater. Chem. 10 (2000) 489–495.
[37] F. Kovanda, T. Rojka, P. Bezdička, K. Jirátová, L. Obalová, K. Pacultovád, Z. Bastl, T. Grygar, J. Solid State Chem. 182 (2009) 27–36.
[38] M.S. Jang, M.K. Yoon, S.H. Lee, H.K. Kim, A. Onodera, S. Kojima, Curr. Appl. Phys. 9 (2009) 651–657.
[39] X. Ni, Q. Zhao, F. Zhou, H. Zheng, J. Cheng, B. Li, J. Cryst. Growth 289 (2006) 299–302.
[40] N. Mironova-Ulmanea, A. Kuzmina, M. Grube, J. Alloys. Compd. 480 (2009) 97–99.
[41] W. Wanga, Y. Liua, C. Xua, C. Zhenga, G. Wanga, Chem. Phys. Lett. 362 (2002) 119–122.
[42] M.H. Chou, S.B. Liu, C.Y. Huang, S.Y. Wu, C.L. Cheng, Appl. Surf. Sci. 254 (2008) 7539–7543.
[43] M.F. Luo, P. Fang, M. He, Y.L.L. Xie, J. Mol. Catal. A: Chem. 239 (2005) 243–248.
[44] M. Jitianu, M. Bălăsoiu, R. Marchidan, M. Zaharescu, D. Crisan, M. Craiu, Int. J. Inorg. Mater. 2 (2000) 287–300.
[45] B. Scheffer, P. Molhoek, J.A. Moullin, Appl. Catal. 46 (1989) 11–30.
[46] S.P. de Lima, V. Vicentini, J.L.G. Fierro, M.C. Rangel, Catal. Today 133–35 (2008) 925–930.
[47] C. Rhodes, G.J. Hutchings, A.M. Ward, Catal. Today 23 (1995) 43–58.